PROCEEDINGS OF SPIE

SPIEDigitalLibrary.org/conference-proceedings-of-spie

Radio frequency shielding of thin aluminized plastic filters investigated for the ATHENA X-IFU detector

Lo Cicero, Ugo, Lo Cicero , Giuseppe, Puccio, Elena, Montinaro, Nicola, Gulli, Daniele, et al.

Ugo Lo Cicero, Giuseppe Lo Cicero , Elena Puccio, Nicola Montinaro, Daniele Gulli, Michela Todaro, Enrico Calandra, Pekka Törmä, Francesco Cuttaia, Fabrizio Villa , Salvatore Ferruggia Bonura , Giuseppe Lullo, Alfonso Collura , Fabio D'Anca, Luisa Sciortino , Salvatore Varisco, Brian Jackson, Bert-Joost van Leeuwen, Emilie Gloaguen, M. Barbera, "Radio frequency shielding of thin aluminized plastic filters investigated for the ATHENA X-IFU detector," Proc. SPIE 10699, Space Telescopes and Instrumentation 2018: Ultraviolet to Gamma Ray, 106994R (6 July 2018); doi: 10.1117/12.2313257

SPIE.

Event: SPIE Astronomical Telescopes + Instrumentation, 2018, Austin, Texas, United States

Radio Frequency shielding of thin aluminized plastic filters investigated for the ATHENA X-IFU detector

Ugo Lo Cicero*[a,b], Giuseppe Lo Cicero[b], Elena Puccio[a], Nicola Montinaro[a], Daniele Gulli[a], Michela Todaro[a], Enrico Calandra[c], Pekka P. Törmä[d], Francesco Cuttaia[e], Fabrizio Villa[e], Salvatore Ferruggia Bonura[b,a], Giuseppe Lullo[c], Alfonso Collura[a], Fabio D'Anca[f], Luisa Sciortino[b], Salvatore Varisco[a], Brian Jackson[g], Bert-Joost van Leeuwen[g], Emilie Gloaguen[h] and M. Barbera[b,a]
[a]Osservatorio Astronomico di Palermo - Istituto Nazionale di Astrofisica (Italy); [b]Dipartimento di Fisica e Chimica - Università degli Studi di Palermo (Italy); [c]Dipartimento di Energia, Ingegneria dell'Informazione e Modelli Matematici - Università degli Studi di Palermo (Italy); [d]AMETEK Finland Oy (Finland); [e]Osservatorio di astrofisica e scienza dello spazio di Bologna - Istituto Nazionale di Astrofisica (Italy); [f]Istituto di BioFisica U.O.S. di Palermo - Consiglio Nazionale delle Ricerche (Italy); [g]SRON Netherlands Institute for Space Research (Netherlands); [h]Ctr. National d'Etudes Spatiales (France)
* ugo.locicero@inaf.it; phone +39 091233621

ABSTRACT

The X-ray Integral Field Unit (X-IFU) is one of the two detectors of the ATHENA astrophysics space mission approved by ESA in the Cosmic Vision 2015-2025 Science Programme. The X-IFU consists of a large array of transition edge sensors (TES) micro-calorimeters covering a field of view of ~5' diameter, sensitive in the energy range 0.2-12 keV, and providing a spectral resolution of 2.5 eV at 7 keV. Both the TES and superconducting quantum interference devices (SQUID) based read-out electronics are very sensitive to electromagnetic interferences (EMI), and a proper shielding of the focal plane assembly (FPA) is required to prevent a deterioration of the energy resolution.

A set of thin filters, highly transparent to X-rays, will be mounted on the FPA and on the cryostat thermal shields in order to attenuate the infrared radiative load, and to protect the detector from contamination. Some of these filters are also aimed at providing proper radio frequency (RF) shielding in the frequency range of the satellite telemetry downlink antenna. In addition, filters should also be effective in shielding any RF interference generated by other on-board electronics. In this paper, we present results from RF measurements performed on thin plastic foils coated with an aluminum layer, with and without metal meshes, and identify the filter characteristics matching the RF shielding requirements.

Keywords: X-ray Integral Field Unit (X-IFU), ATHENA X-ray observatory, EMI shielding, RF attenuation, reverberation chamber, resonance modes, x-ray detectors, thermal thin-film filters.

1. INTRODUCTION

1.1 X-IFU instrument and shielding requirements

ATHENA is the second "L" (Large) space mission selected by the European Space Agency, to be launched by 2030[1]. It will be an X-ray space observatory addressing the Cosmic Vision programme theme "Hot and Energetic Universe". Its aim is to provide both spatially resolved ultra-high-resolution spectroscopy, through the X-ray Integral Field Unit (X-IFU) instrument[2], and wide field spectral imaging, through the Wide Field Imager (WFI) instrument[3]. X-IFU will be sensitive in the 0.2-12 keV energy range, and will achieve unprecedented spectral resolution of 2.5 eV FWHM (full width at half maximum) at 7 keV exploiting highly sensitive transition edge sensors (TES). These operate at a temperature of ~100 mK, thus needing an appropriated multi-stages detector cooling system (DCS). In order to allow the X-rays to reach the detectors, it is necessary to open windows on the cryostat shields and to put filters on these windows to limit the IR thermal load and to reject unwanted radiation[4]. The three outer windows opened in the DCS shields and the associated mechanical supports are named Aperture Cylinder (AC), while the filters, because of their primary role,

Space Telescopes and Instrumentation 2018: Ultraviolet to Gamma Ray, edited by Jan-Willem A. den Herder, Shouleh Nikzad, Kazuhiro Nakazawa, Proc. of SPIE Vol. 10699, 106994R · © 2018 SPIE
CCC code: 0277-786X/18/$18 · doi: 10.1117/12.2313257

are named Thermal Filters (TF). Three TFs will be mounted on the aperture cylinder and two directly on the focal plane assembly (FPA) (Figure 1).

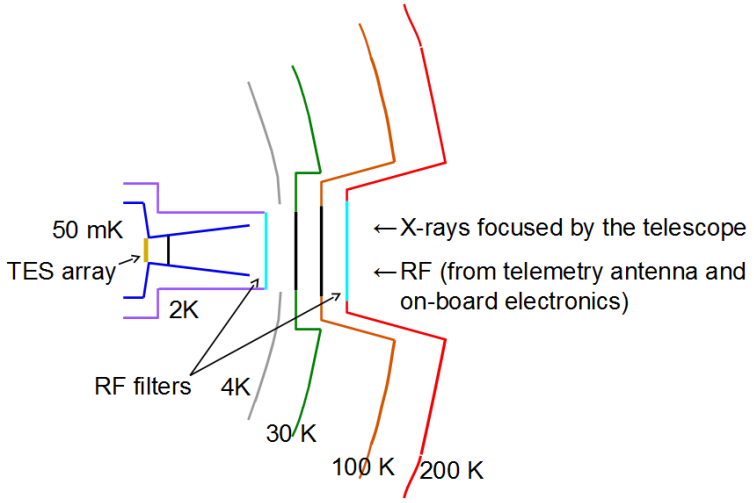

Figure 1. Schematic of the X-IFU cryostat shields (partially shown), the filters (black and cyan) and the TES detector. The two thermal shields at 2 K and 200 K behave also as Faraday cages, so that filters in cyan act as RF shields.

The TFs baseline design, originated by experience from past missions (i.e. Chandra and Astro-H) and based on the X-IFU severe requirements, adopts an aluminum thin film (thickness ~30 nm), supported by a polyimide film (thickness ~45 nm) and a gold-plated stainless steel hexagonal mesh, with pitch in the order of millimeters and thickness of tens to hundreds of microns (Figure 2).

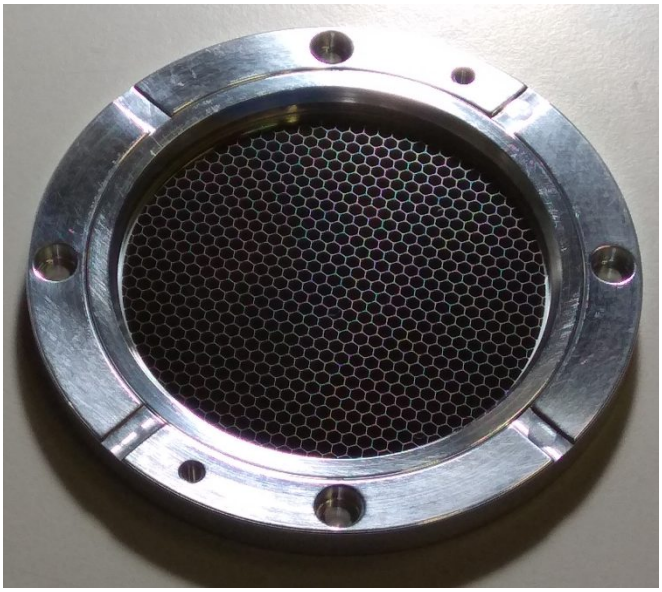

Figure 2. Filter sample. The current baseline specifies 45 nm polyimide film coated with 30 nm Al, supported by a gold plated hexagonal stainless steel mesh.

Part of the unwanted radiation the filters have to reject is the radio frequency (RF) originating from the spacecraft antenna and from the on-board electronics.

In the current baseline design, there are two electromagnetic shields, that coincide with the cryostat shields at 2 K and 200 K. Each of the corresponding TFs, namely TF2 and TF200, has to ensure 30 dB attenuation in the range 30 MHz-18 GHz[5].

In order to properly design the TFs, an extensive characterization campaign is going on, spanning from IR/VIS/UV/X transmission measurements to materials and structural analysis[6]. This work presents the on-going work regarding the characterization of the shielding effectiveness (SE), or RF attenuation, of the filters and their components.

1.2 Measurements in reverberation chamber

The aperture cylinder is a complex electrically large enclosure, meaning that its dimensions are much larger than the free-space wavelengths, at least for the high part of the frequency band of interest. This imply that many electromagnetic modes are supported and many field patterns will be superimposed. The filters SE will be different for each field configuration, because each one will interact differently with the filter materials, so it will depend on the specific AC design. In order to evaluate the filters SE independently from the hosting environment we need to expose them to a great number of field configurations and evaluate the SE statistically.

This kind of measurement method is commonly performed for electromagnetic interference (EMI) studies and carried on in reverberation chambers[7]. As an example, a reverberation chamber setup has been used to evaluate the RF shielding properties of an optically transparent window to be used in infrared sensing systems susceptible to EMI[8].

A reverberation chamber is an enclosure with high RF reflectivity, excited by an input port (e.g. an antenna, a loop, a horn) in which a working volume (WV) exists that presents a statistically homogeneous and uniform field[9]. This field is measured at an output port (e.g. a probe, a horn) placed inside the WV.

The WV properties are obtained by a mechanical or electronic mode-stirring mechanism[10]. The most used methods for mode-stirring involve to continuously change the chamber boundary conditions, either by moving its walls or by means of a moving reflecting structure placed inside the chamber. Another widely used method, the electronic or frequency stirring, consists in exciting the chamber with frequency sweeps, to trigger the resonance of many different modes. For a large enough frequency bandwidth (BW), the statistical parameters (e.g. field average in frequency) will be equivalent to those measured with a mechanical stirrer (e.g. field average in time)[11].

The frequency stirring effectiveness depends on how many modes are excited, that is given by the mode density, function of the chamber geometry, and the excitation frequency, multiplied by the excitation frequency BW[7]. Since we need a SE function of the frequency we need to slice the frequency span of interest in bands thin enough to avoid to smooth out the SE measurement over the frequency, but large enough to excite several modes to obtain an effective stirring. For each band we calculate the statistical properties of choice; for our goal, we choose to evaluate the maximum of the power transmission measured by the output port, to obtain the minimum SE of the filter in the corresponding band.

For both mechanical and frequency stirring the chamber geometry needs to be large enough to support several modes for the lowest frequency of interest. A cylindrical chamber can be seen as part of a circular waveguide closed at the two ends. In a circular waveguide only waves with frequency above the cutoff frequency (f_c) can propagate, since frequencies below f_c are strongly attenuated. The wavelength in the guide (λ_g) is longer than the free space wavelength (λ) and degenerates to infinite at the cutoff frequency.

Transverse magnetic (TM) modes, i.e. electromagnetic waves with the magnetic field laying only on the plane normal to the chamber axis (transverse plane), and transverse electric (TE) modes, with electric field only in the transverse plane, are numbered with subscripts indicating the number of azimuthal and radial variations. The cutoff frequency f_c for the generic TM_{nl} mode is[12]:

$$(f_c)_{TM_{nl}} = \frac{c\, p_{nl}}{\pi\, d} \tag{1}$$

where c is the speed of light, p_{nl} is the l-th root of the n-order Bessel function ($J_n(x) = 0$), and d the guide diameter.

For the generic TE_{nl} mode:

$$(f_c)_{TE_{nl}} = \frac{c\, p'_{nl}}{\pi\, d} \tag{2}$$

where p'_{nl} is the l-th root of the derivative of the n-order Bessel function ($J'_n(x) = 0$).

The wavelength in guide is:

$$\lambda_g = \frac{c}{\sqrt{f^2 - f_c^2}} \tag{3}$$

where f is the frequency and f_c is the cutoff frequency for the mode of interest.

The first mode to propagate (the dominant mode) is the TE_{11} mode (p' = 1.841) and the second is the TM_{01} mode (p = 2.405).

In a cavity, there are further modes (axial modes), usually indicated with a 3rd subscript of the TM_{nl} and TE_{nl} modes, arising from the resonances caused by the superimposition of the waves moving back and forth between the two reflecting end walls. A resonant condition occurs when the length of the cavity is an integer multiple of $\lambda_g/2$:

$$L = m\frac{\lambda_g}{2} \tag{4}$$

where L is the length of the cavity and m is an integer indicating the generic axial mode TE_{nlm} or TM_{nlm}. Combining equations (3) and (4) it is possible to evaluate the maximum number of axial modes m_{max} up to a given frequency:

$$m_{\max} = floor\left(\frac{2L\sqrt{f^2 - f_c^2}}{c}\right) \tag{5}$$

In presence of a conductive filter placed in the middle of the chamber, only even TE axial modes and odd TM axial ones can resonate. The other modes are suppressed by the boundary conditions imposed by the filter itself. These axial modes are the main excited modes in the used reverberation chamber.

2. METHODOLOGY AND SAMPLES

2.1 Instruments and experimental setup

In order to work with a compact setup, we built a 100 mm diameter cylindrical reverberation chamber with a filter holder in the middle and two sliding end walls (Figure 3). It allows to perform both frequency stirring, by frequency sweep excitation, and mechanical stirring, by moving the walls.

The chamber consists in a 0.5 mm thick stainless steel tube with a diameter of 100 mm, closed at its ends by thick aluminum sliding walls. The chosen diameter corresponds to the maximum diameter of the baseline X-IFU filters and is close to the diameter of the smallest cylinder in the AC holding a RF filter. The sliding walls accommodate elastic conductive gaskets to ensure electrical continuity with the tube. The total length of the tube is 900 mm.

The middle section is composed of two flanges, held together by six passing through screws. Filters under test are placed between the flanges. The screws press the flanges on the filter and center it at the same time.

On the sliding walls are mounted the transmitting and the receiving antennas (input and output ports). Each antenna is a brass rod, coaxial to the chamber, with an optional transverse extension to form an “L” shape. Both coaxial and transverse rods are 4 mm in diameter and 40 mm in length.

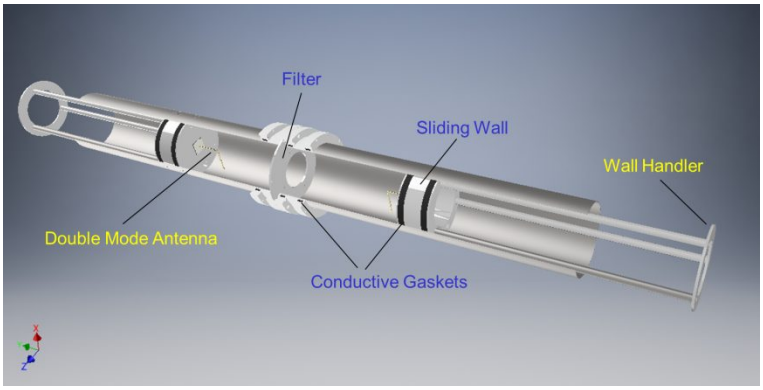

Figure 3. Schematic of the 100 mm diameter reverberation chamber built to perform the SE measurements.

The antennas were connected to the two ports of a Keysight N5232A PNA-L Microwave Vector Network Analyzer (VNA) operating in the frequency range 300 kHz-20 GHz (Figure 4).

The coaxial antenna configuration excites mainly TM modes. Considering the axis-symmetry of the antenna, the main modes excited have no azimuthal variation and one radial variation (TM_{01m} modes). In resonant conditions these modes yield a maximum of electric field at the center of the filter and normal to its plane, maximizing the associated electromagnetic wave transmission.

The "L" shape antenna configuration allows to excite also TE modes. The transverse antenna rod excites mainly modes with one azimuthal and one radial variation (TE_{11m} modes).

Considering the central and symmetric position of the filter, these modes (TE_{11m} and TM_{01m}) should give the maximum RF transmission through the filter.

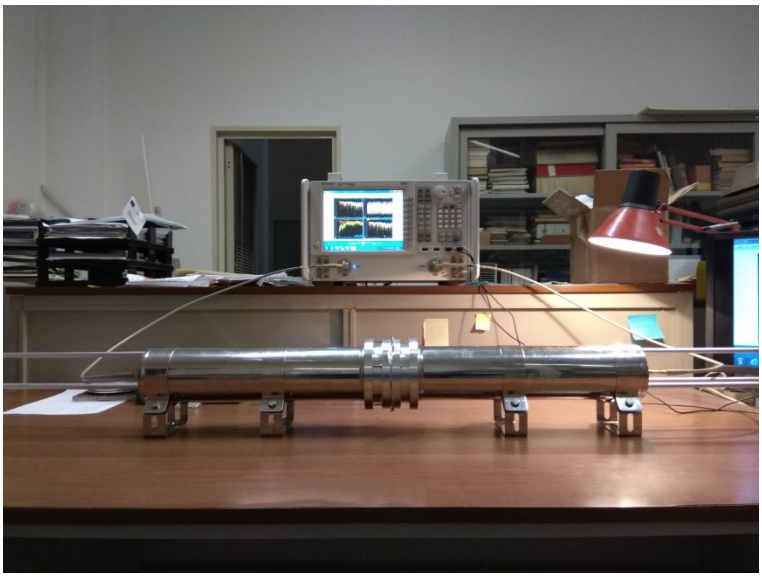

Figure 4. Measurement setup showing the 100 mm diameter reverberation chamber connected to the VNA.

The chamber cutoff frequency for the TE_{11} mode is 1.76 GHz and for the TM_{01} is 2.30 GHz. At the maximum investigated frequency (20 GHz) the chamber could nominally support 61 TE_{nl} and 53 TM_{nl} modes (total 114), but as said, mainly the TE_{11m} and TM_{01m} ones are excited and the others give a minor contribution. From equation (5) and for

the chamber at the maximum extension (internal length 710 mm) it is found that, in the frequency span used for the measurement (0.5-20 GHz), 94 axial modes can be excited for both the TE_{11} and TM_{01} main modes. Equation (5) is valid for an empty cavity therefore minor differences could be found for the real configuration.

2.2 Test samples

The RF attenuation measurements reported in this work were performed on a metal mesh and on aluminum thin film filters. The mesh is hexagonal (honeycomb pattern) and made of copper on FR4 support (fiberglass reinforced resin) (Figure 5). The dimensions are as follows:

- Aperture diameter: 56 mm
- Pitch: 4 mm
- Bars width: 0.2 mm
- Thickness: 35 µm

The mesh is screw-mounted on a 100 mm diameter aluminum ring adapter that can be placed in the measurement setup.

The aluminum filters are made of 90 µm thick Adwill D-675 insulating tape, coated with different thickness of aluminum. They are mounted on 100 mm diameter copper ring frames. The nominal thickness of the aluminum coating for the different filters is 10 nm, 10 nm + 10 nm, 20 nm, 30 nm and 40 nm. The 10 nm + 10 nm filter has a 10 nm coating on both sides of the plastic foil. A non-coated filter was also used as reference (Figure 6).

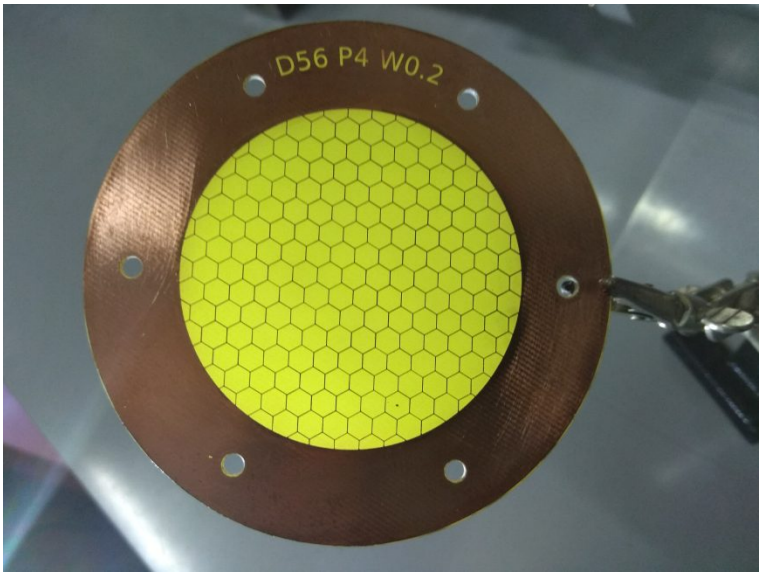

Figure 5. Hexagonal copper mesh on FR4 substrate. Mesh dimensions: diameter 56 mm, pitch 4 mm, thickness 35 µm, bars width 0.2 mm.

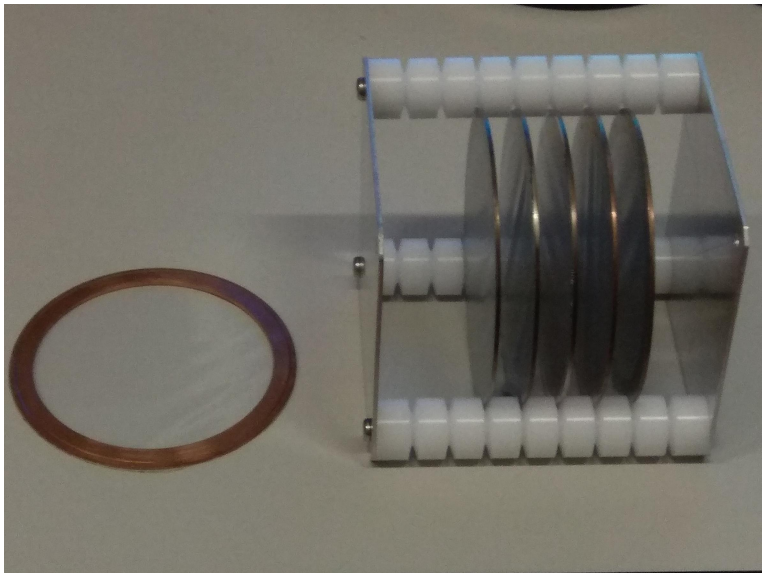

Figure 6. Aluminum thin film filters with different Al coating thickness on insulating tape.

The combinations of every Al filter and the mesh were tested. The mechanical and electrical coupling between mesh and each Al filter was obtained by mounting them on the two sides of a 3 mm thick aluminum disc, with a 56 mm diameter hole. Between mesh and Al filter there is, therefore, a 3 mm gap.

2.3 RF attenuation measurements

The measurements were divided in two sets: the first one with only aluminum coated filters and the second one with the mesh coupled with the aluminum filters. For each set of measurements, a reference without filter and one with a 3 mm thick aluminum disc were measured.

The antennas were mounted in the "L" shape configuration, so both TE and the TM modes were excited. The VNA was calibrated at the antenna connections, using the "SOLT" (Short, Open, Load, Thru) procedure[13].

The VNA settings were:

- Frequency span: 0.5-20 GHz.
- Sweep mode.
- Step: 25 MHz (781 points)
- IF BW: 100 kHz.
- Averaging: 100.
- No smoothing.
- Power: 0 dBm.
- Attenuator: 0 dB.

The described setup can be used with both frequency stirring or mechanical mode stirring, but sliding the cavity walls can cause stress on both connectors and cables connecting the VNA to the antennas, impairing the readings accuracy.

To compare the two stirring methods, a preliminary test at low frequency (up to 3 GHz), with less critical cables and connectors, was performed using an Agilent N9320B Spectrum Analyzer.

The mechanical mode stirring was obtained by slowly sliding the walls while continuously sweeping the frequency. The instrument was set to perform a max hold measurement, meaning that the maximum transmission value for each frequency over all sweeps was saved (max hold in Figure 7).

A frequency mode stirring was also done by sweeping over frequencies without moving the walls (raw data in Figure 7) and evaluating the signal envelope[11]. We evaluated the envelope as the maxima in 400 MHz bands (16 measured points). This BW is large enough so that in the lowest band above cut-off (1.75-2.15 GHz) 6 modes are already supported, and more at higher frequencies.

Both stirring methods provided very similar results (Figure 7), therefore we performed the measurements using only frequency stirring.

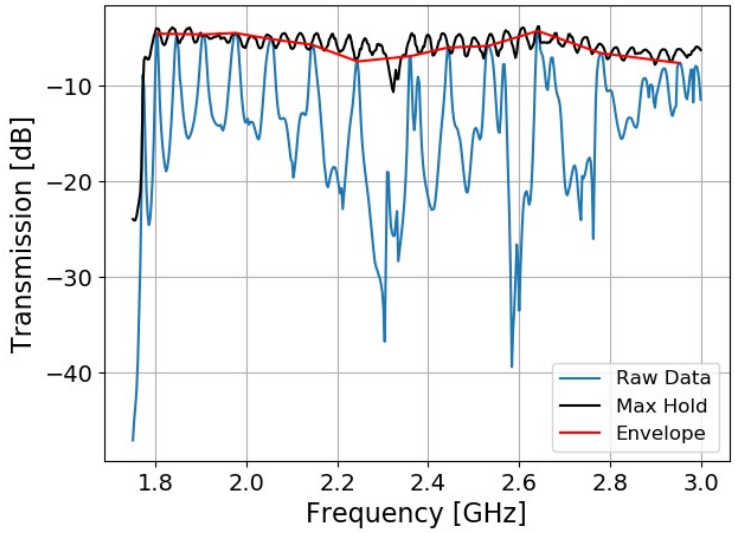

Figure 7. Comparison between SE evaluated by mechanical (max hold) and frequency (envelope) mode stirring, along with single frequency sweep raw data.

3. RESULTS

3.1 Al coating surface resistance

In order to verify the quality of the Al coatings and to extract parameters useful for future simulations, preliminary measurements of the surface resistances were performed. The measurements were done in different zones of the coated surface, using a gold plated 4-point probe and a 4-wire ohm-meter. The surface resistance (R_S) was evaluated averaging the different measurements and using the expression[14]:

$$R_S = R\frac{\pi}{\ln 2} = \frac{\rho}{T} \tag{6}$$

where R is the resistance measured by the ohm-meter, ρ is the resistivity and T the thickness of the conductive coating.

The following values were found (Table 1):

Table 1. Measured values of surface resistance R_S at different nominal thickness Tn of the Al coating.

$\mathbf{T_n}$ [nm]	$\mathbf{R_s}$ [Ω_{sq}]
10	13.0
20	3.76
30	2.04
40	1.41

Aluminum coatings are subject to oxidation when exposed to air. The aluminum oxide has very high resistivity, therefore the conductive thickness of the coating is thinner than the nominal thickness. The resistivity of the conductive part of the coating is usually higher than the resistivity of pure aluminum because the coating is not as compact as the bulk material.

The surface conductance is therefore:

$$G_S = \frac{1}{R_S} = \frac{T}{\rho} = \frac{T_n - T_0}{\rho} \tag{7}$$

Where T_n is the nominal thickness and T_0 is the thickness of the aluminum oxide.

From the model fitting on the measured values the following results were obtained (Figure 8):

- $G_S = 0.021\ T_n - 0.145\ [1/\Omega_{sq}]$
- $\rho = 1 / 0.021 = 47.6\ \Omega \cdot$ nm (pure bulk aluminum: $\rho \sim 28\ \Omega \cdot$ nm)
- $T_0 = 0.145 / 0.021 = 6.9$ nm

The calculated oxide thickness is in good agreement with oxide thickness measurements performed with different methods on Al filter samples[6,15].

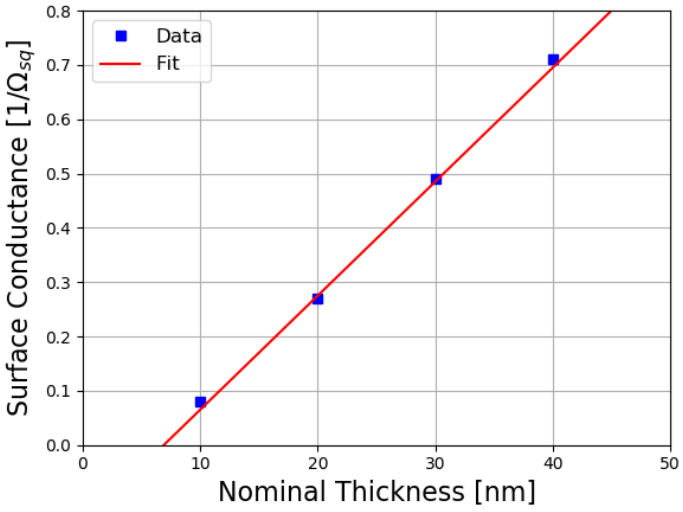

Figure 8. Surface conductance as a function of nominal thickness of the aluminum. The red line represents the model fit, the blue squares the experimental data.

3.2 Shielding effectiveness

Measurements done on aluminum coated filters showed an attenuation increasing with the frequency and the thickness of the coating (Fig. 9). The measurements performed on the two filters with 30 nm and 40 nm of aluminum are very similar, showing that there is not a significant gain in attenuation for aluminum thickness larger than about 30 nm. The plot also shows the open reference attenuation (measurement performed without filters) and the closed configuration (a 3 mm thick aluminum disc placed in the filter holder). The response of the filter with no coating (red curve in Figure 9) is almost identical to the open reference (black line), indicating that the substrate is transparent to the RF. The top profile of the gray area is obtained by adding the open reference attenuation to the required 30 dB attenuation, therefore a curve within the grey area satisfies the attenuation requirement.

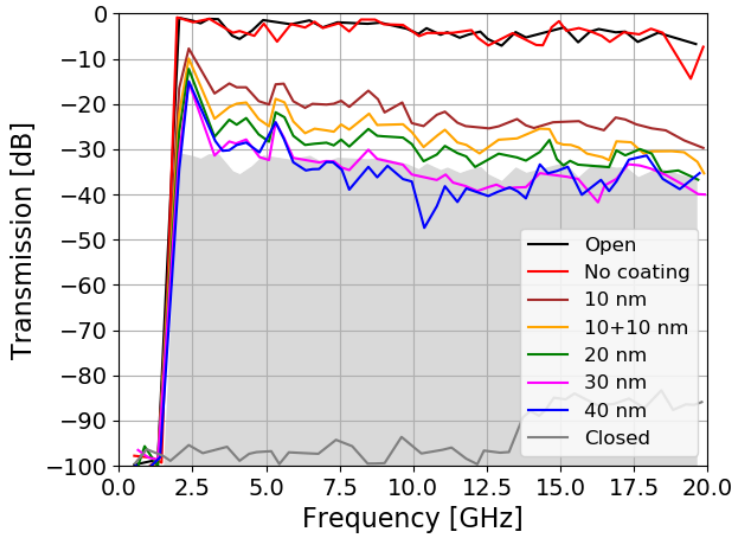

Figure 9. SE of thin Al films with different thickness. “Open” and “Closed” curves show measurements without filters and with a thick Al disk, as references. “No coating” refers to the plastic substrate alone. The gray area displays where requirement is met.

The measurement performed on the mesh showed a higher attenuation at low frequencies (< 7 GHz) (red curve in Figure 10). The attenuation measured at higher frequencies is mainly due to the reduction in diameter from 100 mm of the open configuration (black line in Figure 10) to 56 mm diameter of the copper mesh (red line in Figure 10) and likely not due to the mesh itself. Coupling the two kinds of filters together, there is a compensation of the different behaviors, improving the overall performance. The gray area in the plots shows where the requirement is satisfied, as in Figure 9.

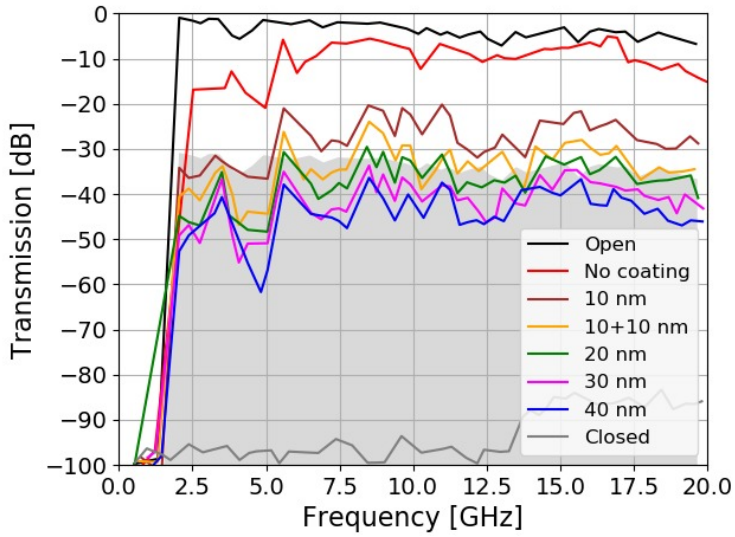

Figure 10. SE of the copper mesh combined with different Al films, along with references (as in Figure 9). In red the SE of the mesh alone. In gray the area where the requirement is met.

Effective SE is obtained by subtracting the open reference attenuation to that of the filter. Minimum attenuations obtained in 400 MHz bands, centered at the specified frequencies, are shown in Table 2. The table reports both attenuations of the aluminum filters alone and the combinations of those filters with the mesh.

Table 2. Attenuation values obtained for Al filters alone and with mesh at different frequencies.

Attenuation [dB]								
Frequency [GHz]	**2.4**		**6**		**10**		**18**	
Al coating [nm]	**No mesh**	**mesh**	**No mesh**	**mesh**	**No mesh**	**mesh**	**No mesh**	**mesh**
0	0	15	0	11	0	4	0	6
10	6	35	17	31	21	19	21	25
10+10	8	37	22	37	23	26	26	30
20	11	45	25	41	25	29	26	33
30	14	45	30	43	32	34	30	36
40	13	48	31	45	34	37	27	39

4. CONCLUSIONS

We investigated the shielding effectiveness of the X-IFU thermal filters also devoted to the attenuation of the radio frequency entering the aperture cylinder. In order to expose the filters to different electromagnetic field distributions, we built a reverberation chamber able to perform RF attenuation measurements with both mechanical and frequency mode stirring.

We performed the RF attenuation measurements on a set of aluminum thin-films with thickness in the range 10-40 nm supported by plastic foils, on a hexagonal copper mesh with 4 mm pitch and 0.2 mm bars width, and on the combinations between Al films and the mesh.

We found that the mesh exhibits a good attenuation below 7 GHz and the aluminum filters perform better at higher frequencies. The combination of the mesh coupled with the aluminum filters showed a compensation of the two opposite behaviors, providing a good attenuation in the whole frequency range of interest. In particular, coupling the mesh with a 30 nm thick aluminum filter, the measured RF attenuation is higher than 30 dB and thus compatible with requirements.

We also performed a characterization of the surface resistance of aluminum coatings of different thicknesses, which allowed us to derive the resistivity of deposited aluminum as well as the aluminum oxide thickness. These results gave information on the quality of the coatings and will be useful for the on-going FEM RF modelling.

We plan to continue this activity by measuring the RF attenuation of meshes with different geometrical parameters (pitch and bar width) in order to identify the proper geometry for the design of optimized meshes of the two X-IFU thermal filters mounted on Faraday cages, namely TF2 and TF200.

The overall attenuation of the full set of TFs strongly depends on the environment of the aperture cylinder and focal plane assembly (e.g. geometry, surface treatment, etc.); for this reason, we will complement the measurements performed so far on individual filters with simulations as well as new measurements of a simplified mock-up of the AC and FPA shields with representative TFs in place.

ACKNOWLEDGMENTS

The research leading to these results has received funding from the European Union's Horizon 2020 Program under the AHEAD project (grant agreement n. 654215), and from ESA (European Space Agency) under the contract n. 4000120250/17/NL/BJ. We acknowledge fruitful discussions with Jean Michel Mesnager and Philippe Peille of CNES (FR), and Roland den Hartog of SRON (NL).

REFERENCES

[1] Barcons, X., Nandra, K., Barret, D., Den Herder, J.-W., Fabian, A. C., Piro, L., Watson, M. G. and the Athena team, "Athena: the X-ray observatory to study the hot and energetic Universe," J. Phys.: Conf. Ser. 610, 012008, 1-8 (2015). https://doi.org/10.1088/1742-6596/610/1/012008.

[2] Barret, D., Trong, T. L., den Herder, J. W., Piro, L., Barcons, X., Huovelin, J., ... & Rauw, G., "The Athena X-ray Integral Field Unit (X-IFU)," Proc. SPIE, Space Telescopes and Instrumentation 2016: Ultraviolet to Gamma Ray, 9905, 99052F, (2016). https://doi.org/10.1117/12.2232432.

[3] Meidinger, N., Barbera, M., Emberger, V., Fürmetz, M., Manhart, M., Müller-Seidlitz, J., Nandra, K., Plattner, M., Rau, A., Treberspurg, W., "The Wide Field Imager instrument for Athena," Proc. SPIE, UV, X-Ray, and Gamma-Ray Space Instrumentation for Astronomy XX, 10397, 103970V (2017). https://doi.org/10.1117/12.2271844.

[4] Barbera, M., Argan, A., Bozzo, E., Branduardi-Raymont, G., Ciaravella, A., Collura, A., Cuttaia, F., Gatti, F., Jimenez Escobar, A., Lo Cicero, U., Lotti, S., Macculi, C., Mineo, T., Nuzzo, F., Paltani, S., Parodi, G., Piro, L., Rauw, G., Sciortino, L., Sciortino, S. Villa, F., "Thermal Filters for the ATHENA X-IFU: Ongoing Activities Toward the Conceptual Design," J. Low Temp. Phys. 184, 706–711 (2016). https://doi.org/10.1007/s10909-016-1501-4.

[5] "X-IFU Optical Thermal blocking Filter requirements document," XIFU-RD-10000-00347-CNES (Private communication – draft).

[6] Barbera et Al., "Development status of the ATHENA X-IFU thermal filters toward the end of phase A," these proceedings, 10699-62 (2018).

[7] Holloway, C. L., Hill, D. A., Sandroni, M., Ladbury, J. M., Coder, J., Koepke, G., Marvin, A. C., He, Y., "Use of Reverberation Chambers to Determine the Shielding Effectiveness of Physically Small, Electrically Large Enclosures and Cavities," IEEE Trans. Electromagn. Compat. 50, 770-782 (2008). https://doi.org/10.1109/TEMC.2008.2004580.

[8] Savrun, E., and H. Del Aguila. "Electrically conductive tungsten silicide coatings for EMI/RFI shielding of optically transparent windows," J. Mater. Sci. 33, 2893-2897 (1998). https://doi.org/10.1023/A:1017554307521.

[9] Leferink, F.B.J., Bergsma, H. Van Etten, W. C., "Shielding Effectiveness Measurements using a Reverberation Chamber," Symp. Rec. - IEEE Int. Symp. Electromagn. Compat. 505-508 (2006). https://doi.org/10.1109/EMCZUR.2006.214982.

[10] Serra, R., Marvin, A. C., Moglie, F., Primiani, V. M., Cozza, A., Arnaut, L. R., Huang, Y., Hatfield, M., Klingler, M., and Leferink, F. "Reverberation Chambers à la carte: An overview of the different mode-stirring techniques," IEEE Electromagn. Compat. Magazine 6, 63-78 (2017). https://doi.org/10.1109/MEMC.2017.7931986.

[11] Hill, D. A. "Electronic mode stirring for reverberation chambers," IEEE Trans. Electromagn. Compat. 36, 294-299 (1994). https://doi.org/10.1109/15.328858.

[12] Ramo, S., Whinnery, J. R., Van Duzer, T. [Fields and Waves in Communications Electronics], John Wiley and Sons, Inc., New York, London, Sydney, 429-439 (1965).

[13] Agilent Technologies, [Advanced Calibration Techniques for Vector Network Analyzers] Modern Measurement Techniques for Testing Advanced Military Communications and Radars, 2nd Edition © Agilent Technologies, Inc. (2006).

[14] Smits, F. M. "Measurement of sheet resistivities with the four-point probe," Bell Syst. Tech. J. 37, 711-718 (1958). https://doi.org/10.1002/j.1538-7305.1958.tb03883.x

[15] Sciortino, L., Lo Cicero, U., Magnano, E., Píš, I. and Barbera, M. "Surface investigation and aluminum oxide estimation on test filters for the ATHENA X-IFU and WFI detectors," Proc. SPIE, Space Telescopes and Instrumentation 2016: Ultraviolet to Gamma Ray, 9905, 990566, (2016). https://doi.org/10.1117/12.2232376.